Electronic Supplementary Material (ESI) for Inorganic Chemistry Frontiers.

Supporting Information

Mechanistic insights into dual active sites in Au@$W_{18}O_{49}$ electrocatalysts for hydrogen evolution reaction

Yaqin Yu[a, b], Zhen Zhou[c], Xiaoping Song[a], Xiaowei Song[a], Zhengdong Zhang[a,*], Chuanyong Jing[b,*]

[a] *Center for Environmental Metrology, National Institute of Metrology, Beijing 100085, China.*

[b] *State Key Laboratory of Environmental Chemistry and Ecotoxicology, Research Center for Eco-Environmental Sciences, Chinese Academy of Sciences, Beijing 100085, China*

[c] *State Key Laboratory of Technologies in Space Cryogenic Propellants, Beijing Special Engineering Design and Research Institute, Beijing 100028, China*

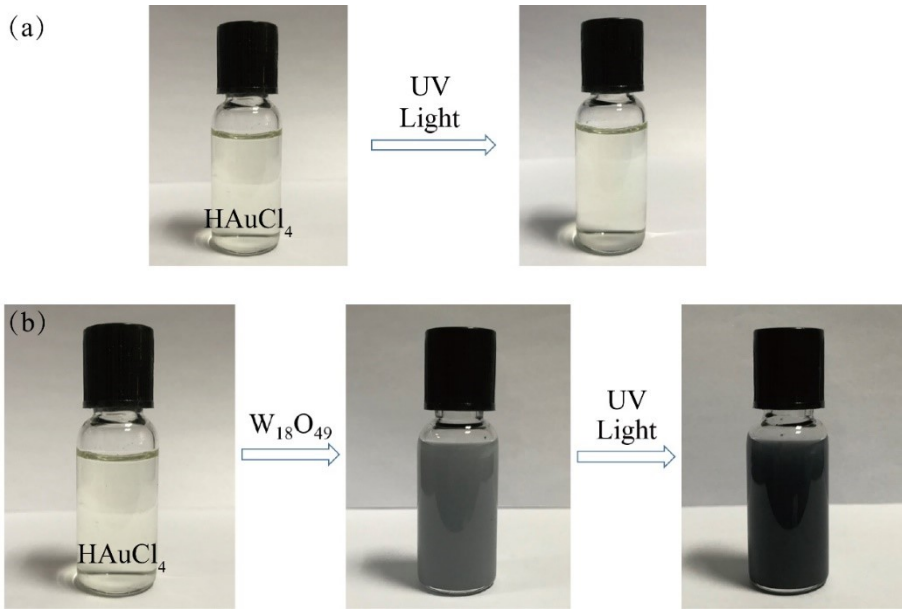

Figure S1 Pictures of (a) $HAuCl_4$ solution under UV irradiation and (b) mixed solution of $HAuCl_4$ and $W_{18}O_{49}$ under UV irradiation.

SERS measurement

A mixture containing 10^{-5} M R6G and 0.1 $g \cdot L^{-1}$ Au@$W_{18}O_{49}$ was dropped on silicon wafers and detected by the state translation nanoparticle-enhanced Raman spectroscopy (STNERS) method. Raman spectra were collected on a laser confocal microscopy Raman spectrometer (LabRAM HR Evolution, HORIBA, JPN) with an excitation wavelength of 785 nm. The spectra were acquired for 10 s with three accumulations.

Fig. S2a shows the Raman spectra of R6G (10^{-5} M) on the surface of Au@$W_{18}O_{49}$ synthesized at different UV irradiation times. A significant Raman enhancement was observed by extending the UV irradiation time. Four characteristic bands of R6G centered at 612, 773, 1360, and 1650 cm^{-1}, named P1, P2, P3, and P4, were detected, suggesting that Au@$W_{18}O_{49}$ could work as SERS substrates. The Raman intensity of R6G as a function of UV irradiation time (Fig. S2b) suggests that the adsorbed $AuCl_2$ molecules were reduced to Au NPs at twelve minutes. With the irradiation time extending to about 18 minutes, the size and gaps of Au nanoparticles were optimal.

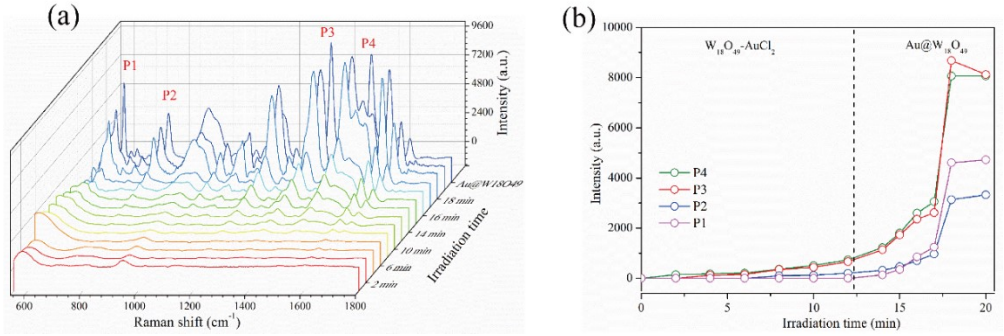

Figure S2 (a) Surface-enhanced Raman spectra of R6G with Au@$W_{18}O_{49}$ as substrates, and (b) intensity of R6G Raman peaks with extending UV irradiation time.

Characterization of Au@$W_{18}O_{49}$ catalysts

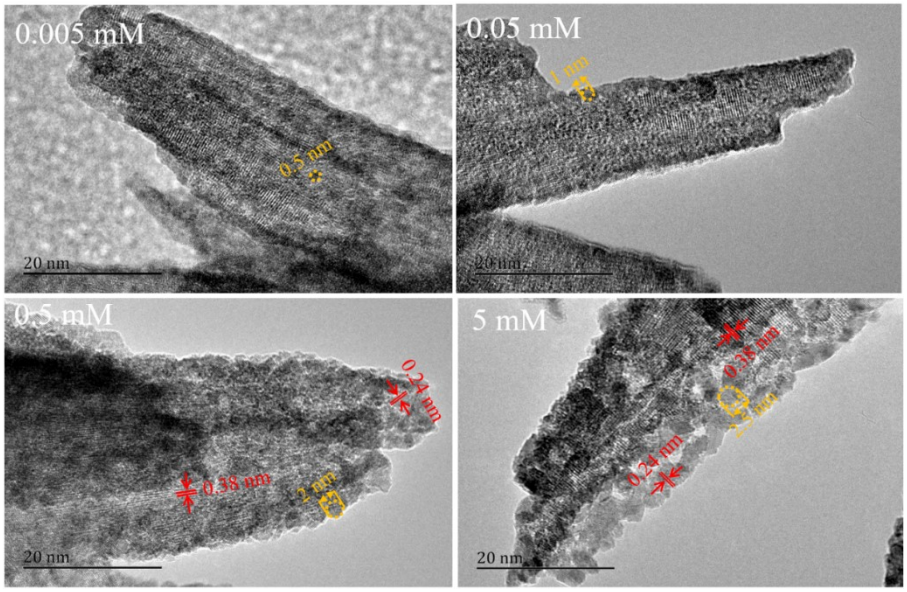

Figure S3 HR-TEM images of Au@$W_{18}O_{49}$ synthesized with 0.005, 0.05, 0.5, and 5 mM $HAuCl_4$ solution.

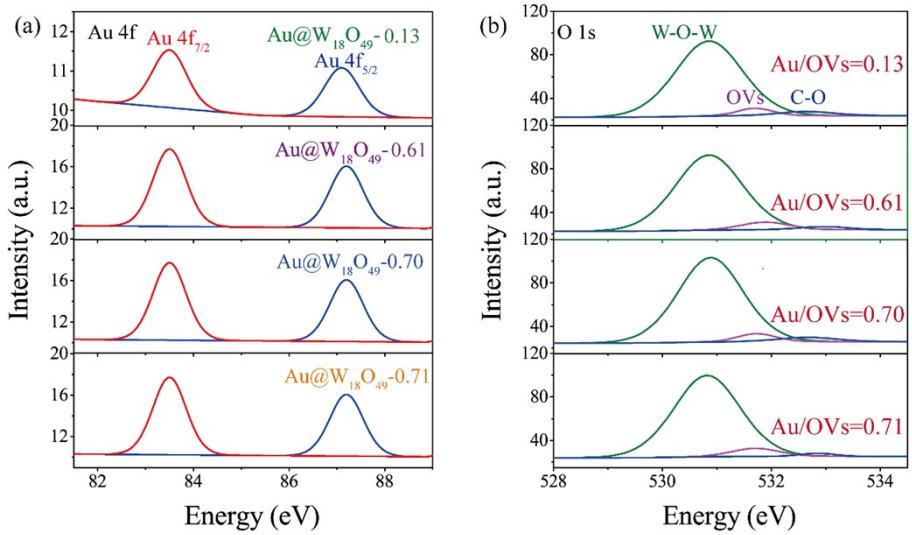

Figure S4 XPS Au4f spectra (a) and O1s spectra (b) of Au@$W_{18}O_{49}$-0.13, Au@$W_{18}O_{49}$-0.61, Au@$W_{18}O_{49}$-0.70, andAu@$W_{18}O_{49}$-71.

The Brunauer–Emmett–Teller (BET) specific surface area was determined from the N_2 adsorption-desorption isotherms obtained using an automated gas sorption instrument (Quantachrome Instruments, US).

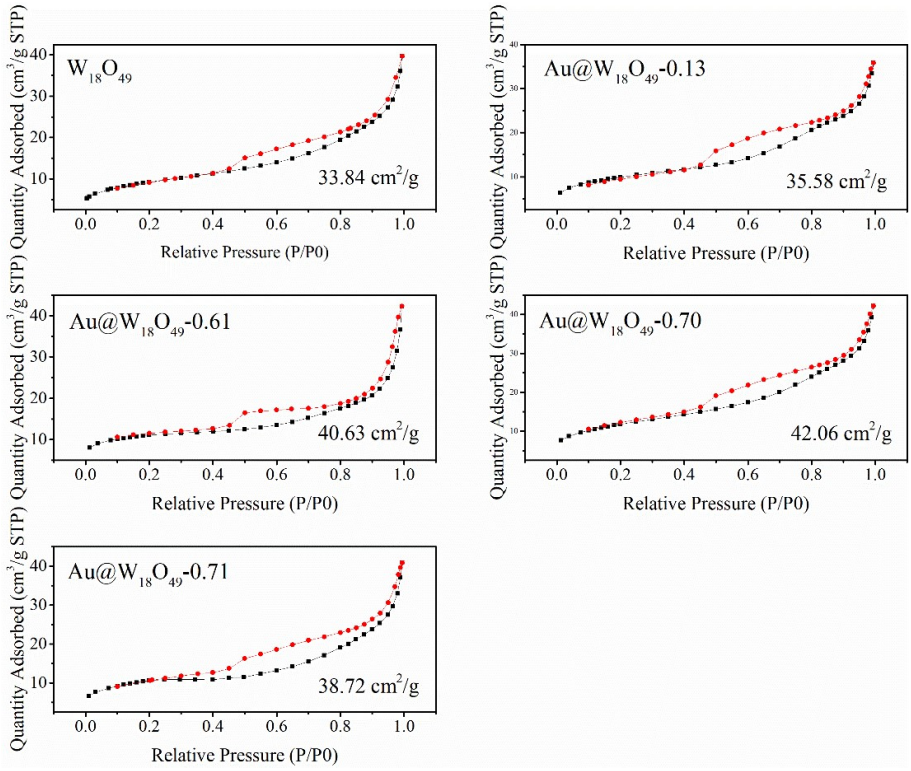

Figure S5 N_2 adsorption-desorption isotherms of $W_{18}O_{49}$, Au@$W_{18}O_{49}$-0.13, Au@$W_{18}O_{49}$-0.61, Au@$W_{18}O_{49}$-0.70, Au@$W_{18}O_{49}$-0.71.

Electrochemical Behavior of $Au@W_{18}O_{49}$

The catalytic performance of the prepared samples for hydrogen evaluation reaction was measured with a three-electrode cell by linear sweep voltammetry on an Autolab electrochemical analyzer (PGSTAT302N, Switzerland). A commercial glassy carbon electrode (GCE) served as the working electrode, graphite rod electrode as the counter electrode, and Ag/AgCl (CH Instruments, Shanghai, China) as the reference electrode. The commercial GCE (~0.07 cm^2 area, 3 mm diameter) was polished with alumina powder, ultrasonically washed, and blow-dried. About 5 mg of the measured materials were dispersed in the mixture solution of 0.2 mL 5 wt% Nafion solution and 1.8 mL ethanol by ultrasonication for 30 min to obtain a homogeneous solution. Then, 5 μL of the as-prepared ink was dropped on the polished GCE (mass loading ≈ 0.17 mg cm^{-2}). The electrolyte (0.5 M H_2SO_4) was purged with H_2 gas for at least 30 min to reach the H_2O/H_2 equilibrium.

HER polarization curve was recorded between 0.1 and -0.8 V versus the reversible hydrogen electrode (RHE) at the scan rate of 5 $mV \cdot s^{-1}$. The polarization curves were measured with an ohmic potential drop (iR) correction. Tafel plots of the linear region were obtained using the following Tafel equation: $\eta=a+b\times\log j$, where η represents overpotential, b is the Tafel slope, and j represents the current density. For iR compensation, the potential was corrected according to the equation: $E_{com}=E_{mea}-iR_u$, where E_{com} is the compensated potential, E_{mea} is the measured potential, i is the current, and R_u stands for the series resistance based on electrochemical impedance spectroscopy (EIS) measurements. EIS was conducted under a potential of −0.160 V (vs RHE) in the frequency range of 100 kHz to 0.1 Hz with 5 mV amplitude. The Faradic efficiency of HER catalysts is defined as the ratio of the amount of experimentally determined H_2 to that of the theoretically expected H_2 from the reaction. and S10). The amount of H_2 evolved during HER was determined quantitatively by gas chromatography (GC-2030ATF, SHIMADZU). The theoretical amount of H_2 can be calculated using the following formula: $M = (I \times t) / (n \times F)$, where I represents the current (mA), t is the electrolysis time (s), n indicates the number of electrons

transferred (n= 2 for the HER), F is the Faraday constant (96,485C mol^{-1}).

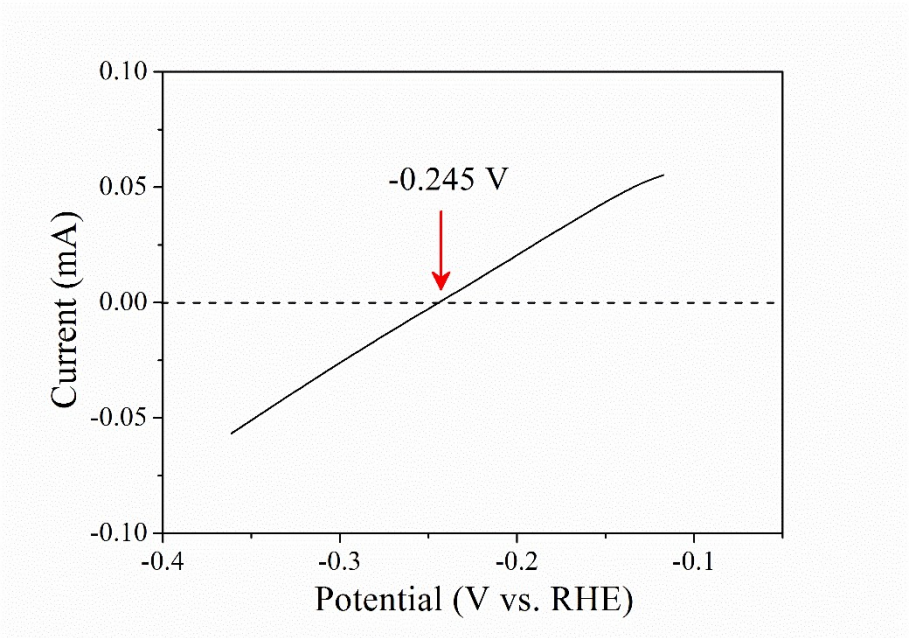

Figure S6 Current-potential curve for the calibration of Ag/AgCl electrode with respect to RHE in 0.5 M H_2SO_4 with a glassy carbon electrode as the working electrode.

As shown in Fig. S7, the peak current increased linearly with the scan rate increasing from 20 to 100 $mV \cdot s^{-1}$. The CV spectra conform to the Randles-Sevcik equation, $i_p = (2.69 \times 10^5) n^{3/2} A C D^{1/2} v^{1/2}$. In the equation, i_p=maximum current, n=number of electrons, A=electrode area, C=$K_3[Fe(CN)_6]$ concentration, D=diffusion coefficient, v=scan rate.

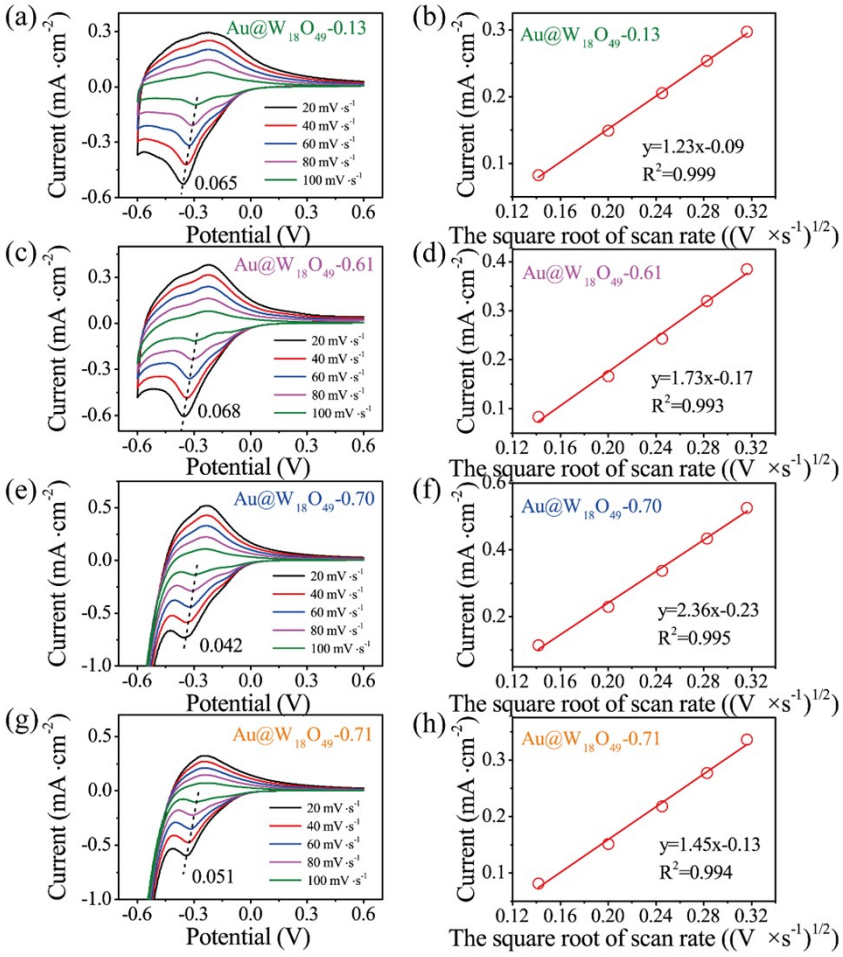

Figure S7 Cycle voltammogram for (a) Au@$W_{18}O_{49}$-0.13, (c) Au@$W_{18}O_{49}$-0.61, (e) Au@$W_{18}O_{49}$-0.70, and (g) Au@$W_{18}O_{49}$-0.71 with scan rate increasing from 20 to 100 $mV \cdot s^{-1}$. (b), (d), (f), and (h) The corresponding linear relationship between current versus the square root of scan rate.

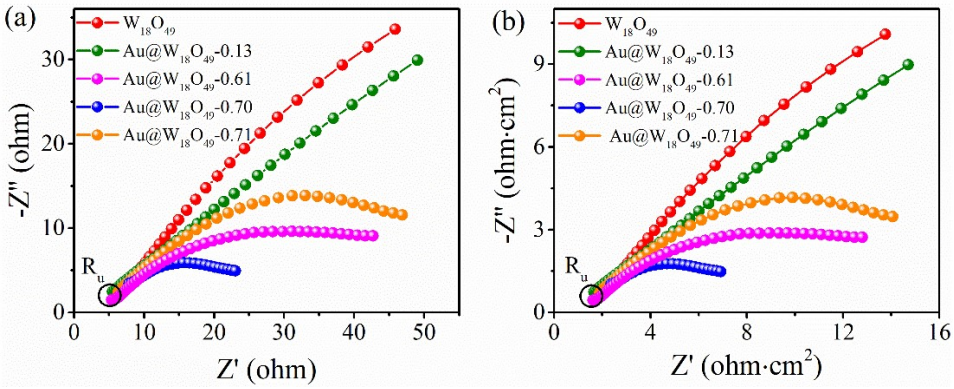

Figure S8 Nyquist plot of Au@$W_{18}O_{49}$ acquired in 0.5 M H_2SO_4 from 100 kHz to 0.1 Hz without (a) and with (b) geometrical area normalization.

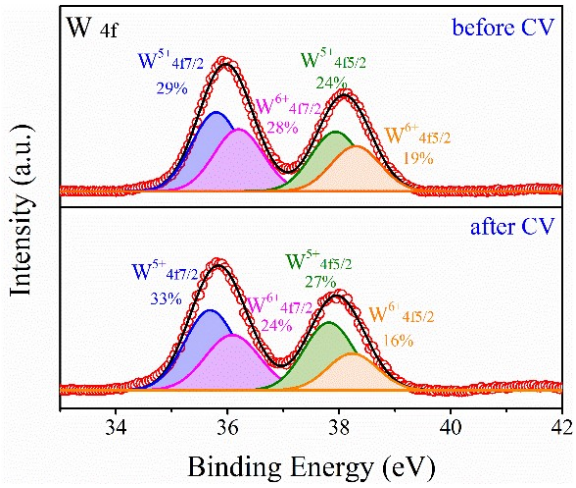

Figure S9 XPS W 4f spectra of Au@$W_{18}O_{49}$-0.70 before and after long-term potential cycling.

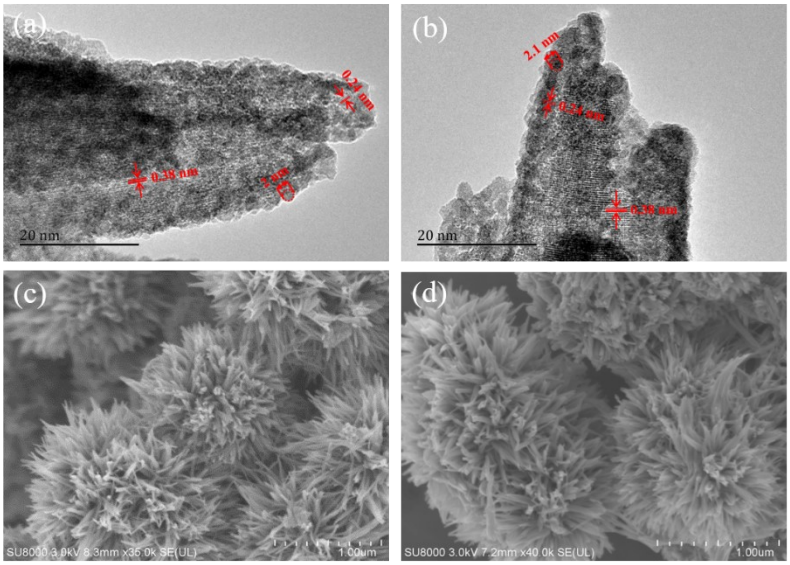

Figure S10 HR-TEM images of Au@$W_{18}O_{49}$-0.70 (a) before and (b) after long-term potential cycling. SEM images of Au@$W_{18}O_{49}$-0.70 (c) before and (d) after long-term potential cycling.

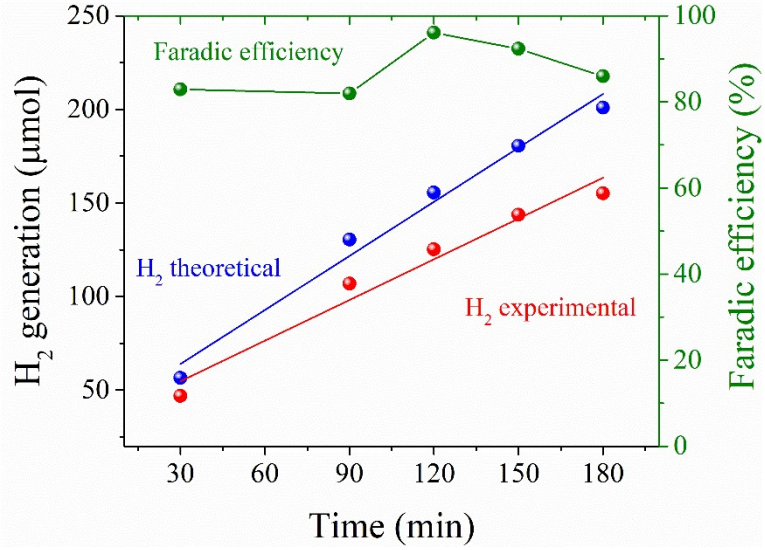

Figure S11 Amount of H_2 theoretically calculated and experimentally measured as a function of time. The Faradic efficiency of Au@$W_{18}O_{49}$-0.70 catalysts in 0.5 M H_2SO_4.

Table S1. Comparison of η_{10} and Tafel slope for the HER of Au@$W_{18}O_{49}$ catalysts.

Sample	η_{10} (mV)	Tafel slope (mV·dec^{-1})
$W_{18}O_{49}$	507±18.9	163±16.2
Au@$W_{18}O_{49}$-0.13	492±19.1	153±10.2
Au@$W_{18}O_{49}$-0.61	94±25.2	76±3.7
Au@$W_{18}O_{49}$-0.70	79±18.1	58±3.0
Au@$W_{18}O_{49}$-0.71	302±37.8	92±1.5

Table S2. Comparison of η_{10} and Tafel slope for the HER of prepared and reported WO_x-based catalysts.

Electrodes	**η_{10} (mV)**	**Tafel slope (mV·dec^{-1})**	**C_{dl} (mF·cm^{-2})**	**Ref.**
WO_3 spheres	520	139	-	[1]
WO_x-PtNi@Pt DNWs	22	-	-	[2]
Pt NP/WO_{3-x}	38	-	-	[3]
Pt/def-WO_3@CFC	42	61	36.3	[4]
Meso-WO_3	598	134	-	[5]

Meso-$WO_{2.83}$	287	95	-	[5]
Pt-WO_x/WS_2	42	26	4.16	[6]
WOx/C-4	202.60	198.26	-	[7]
WO_3 nanorods	152	96	1.05	[8]
WS_2/WO_3	395	50	-	[9]
Ni_2P-WO_3-60	105	92	0.23	[10]
m-WO_3/rGO	35	32	-	[11]
h-WO_3/rGO	69	37	-	[11]
Monoclinic-WO_3	106	78	0.062	[12]
Hexagonal-WO3	83	48	0.152	[12]
WO_{3-x}-30-CNFs	185	89	711	[13]
Mo-$W_{18}O_{49}$	45	54	5.9	[14]
Pd- $W_{18}O_{49}$	137	54	-	[15]
WO_2-MWCMN	58	46	-	[16]
Pt/C	34	46	-	
Au@$W_{18}O_{49}$-0.70	**79**	**58**	**3.9**	

Table S3. Comparison of η_{10} and Tafel slope for the HER of prepared and reported Au-based catalysts.

Electrodes	**η_{10} (mV)**	**Tafel slope (mV·dec^{-1})**	**C_{dl} (mF·cm^{-2})**	**Ref.**
Au/Co_3O_4	168	79	-	[17]
Au/Ni_3S_2	97	51	18.5	[18]
Au@$Co_2N_{0.67}$/3D-NGr	91.4	52.3	24.1	[19]
Au/MoS_2	77	92	11.1	[20]
MoS_2/Au^0/N-CNT	318	128	37	[21]
Au-MoS_2/CNFs	92	126	14.4	[22]
3DG-Au-Ni_3S_2-15c	140	93	37.98	[23]
Au/rGO	176	88	-	[24]

S-Au@MoS_2	164	50	-	[25]
Au-MoS_2	120	163	-	[26]
MoS_2-Au	66	40	-	[27]
Au@NC	130	76.8	18.65	[28]
Au/rGO	260	39.2	-	[29]
C/Ni-AuPt	131	66	0.828	[30]
AuRu alloy NFs	43	35.7	-	[31]
Au NDs	67	65	-	[32]
Au/Co_9S_8	35	64	9.8	[33]
Au-SnO_x	148	79	0.017	[34]
TiO_2 NBs@TiO_2 NSs@Au NPs	440	58	0.026	[35]
Au/Cu-NPZ-CPE	100	33	12.9	[36]
Au-Cu/CNFs	83	70	483	[37]
Pt-Au NPs/CNFs	235	84	-	[38]
AuNPs@NCNRs/CNFs	126	93	-	[39]
Au@$W_{18}O_{49}$-0.70	**79**	**58**	**3.9**	

References

1. M. M. Mohamed, T. M. Salama, M. A. Hegazy, R. M. Abou Shahba and S. H. Mohamed, Synthesis of hexagonal WO_3 nanocrystals with various morphologies and their enhanced electrocatalytic activities toward hydrogen evolution, *Int. J. Hydrogen Energy*, 2019, **44**, 4724-4736.
2. W. Zhang, B. Huang, K. Wang, W. Yang, F. Lv, N. Li, Y. Chao, P. Zhou, Y. Yang, Y. Li, J. Zhou, W. Zhang, Y. Du, D. Su and S. Guo, WO_x-surface decorated PtNi@Pt dendritic nanowires as efficient pH-universal hydrogen evolution electrocatalysts, *Adv. Energy Mater.*, 2021, **11**.
3. J. Park, S. Lee, H. Kim, A. Cho, S. Kim, Y. Ye, J. W. Han, H. Lee, J. H. Jang and J. Lee, Investigation of the support effect in atomically dispersed Pt on WO_{3-x} for utilization of Pt in the hydrogen evolution reaction, *Angew. Chem. Int. Ed.*, 2019, **58**, 16038-16042.
4. H. Tian, X. Z. Cui, L. M. Zeng, L. Su, Y. L. Song and J. L. Shi, Oxygen vacancy-assisted hydrogen evolution reaction of the Pt/WO_3 electrocatalyst, *J. Mater. Chem. A*, 2019, **7**, 6285-6293.
5. H. Cheng, M. Klapproth, A. Sagaltchik, S. Li and A. Thomas, Ordered mesoporous $WO_{2.83}$:

selective reduction synthesis, exceptional localized surface plasmon resonance and enhanced hydrogen evolution reaction activity, *J. Mater. Chem. A*, 2018, **6**, 2249-2256.

6. L. S. Oh, J. Y. Kim, H. W. Kim, J. Han, E. Lim, W. B. Kim, J. H. Park and H. J. Kim, Unveiling the enhanced electrocatalytic activity at electrochemically synthesized Pt-WOx hybrid nanostructure interfaces, *Chem. Commun.*, 2021, **57**, 11165-11168.
7. J. Lu, G. Qian, L. Luo, H. He and S. Yin, Contributions of oxygen vacancies to the hydrogen evolution catalytic activity of tungsten oxides, *Int. J. Hydrogen Energy*, 2021, **46**, 676-682.
8. R. Rajalakshmi, A. Rebekah, C. Viswanathan and N. Ponpandian, Evolution of intrinsic 1-3D WO_3 nanostructures: Tailoring their phase structure and morphology for robust hydrogen evolution reaction, *Chem. Eng. J.*, 2022, **428**.
9. X. Shang, Y. Rao, S. Lu, B. Dong, L. Zhang, X. Liu, X. Li, Y. Liu, Y. Chai and C. Liu, Novel WS_2/WO_3 heterostructured nanosheets as efficient electrocatalyst for hydrogen evolution reaction, *Mater. Chem. Phys.*, 2017, **197**, 123-128.
10. B. Wang, L. Wang, Y. Qian, Y. Yang, T. T. Isimjan and X. Yang, Construction of a self-supporting Ni_2P-WO_3 heterostructure for highly efficient hydrogen evolution under both caustic and acidic conditions, *Sustain. Energy Fuels*, 2021, **5**, 2884-2892.
11. J. Yang, X. Chen, X. Liu, Y. Cao, J. Huang, Y. Li and F. Liu, From hexagonal to monoclinic: engineering crystalline phase to boost the intrinsic catalytic activity of tungsten oxides for the hydrogen evolution reaction, *ACS Sustain. Chem. Eng.*, 2021, **9**, 5642-5650.
12. X. Zhang, G. Jin, D. Wang, Z. Chen, M. Zhao and G. Xi, Crystallographic phase and morphology dependent hydrothermal synthesis of tungsten oxide for robust hydrogen evolution reaction, *J. Alloys Compd.*, 2021, **875**.
13. J. D. Chen, D. N. Yu, W. S. Liao, M. D. Zheng, L. F. Xiao, H. Zhu, M. Zhang, M. L. Du and J. M. Yao, WO_{3-x} nanoplates grown on carbon nanofibers for an efficient electrocatalytic hydrogen evolution reaction, *ACS Appl. Mater. Interfaces*, 2016, **8**, 18132-18139.
14. X. Zhong, Y. Sun, X. Chen, G. Zhuang, X. Li and J. Wang, Mo doping induced more active sites in urchin-like $W_{18}O_{49}$ nanostructure with remarkably enhanced performance for hydrogen evolution reaction, *Adv. Funct. Mater.*, 2016, **26**, 5778-5786.
15. Y. Y. Zhao, Q. W. Tang, P. Z. Yang and B. L. He, Robust electrocatalysts from metal doped $W_{18}O_{49}$ nanofibers for hydrogen evolution, *Chem. Commun.*, 2017, **53**, 4323-4326.
16. R. Wu, J. F. Zhang, Y. M. Shi, D. Liu and B. Zhang, Metallic WO_2-carbon mesoporous nanowires as highly efficient electrocatalysts for hydrogen evolution reaction, *J. Am. Chem. Soc.*, 2015, **137**, 6983-6986.
17. X. L. Zhong, J. Z. Huang, M. Wang and L. S. Wang, Polythionine coated on Au/Co_3O_4 enhances the performance for hydrogen evolution reaction, *NANO*, 2021, **16**.
18. H. Liu, J. N. Cheng, W. J. He, Y. Li, J. Mao, X. R. Zheng, C. Chen, C. X. Cui and Q. Y. Hao, Interfacial electronic modulation of Ni_3S_2 nanosheet arrays decorated with Au nanoparticles boosts overall water splitting, *Appl. Catal. B-Environ.* 2022, **304**.
19. D. C. Nguyen, T. L. L. Doan, S. Prabhakaran, D. H. Kim, N. H. Kim and J. H. Lee, Rational construction of Au@$Co_2N_{0.67}$ nanodots-interspersed 3D interconnected N-graphene hollow sphere network for efficient water splitting and Zn-air battery, *Nano Energy*, 2021, **89**.
20. Y. T. Jing, R. J. Wang, Q. Wang and X. F. Wang, Gold nanoclusters grown on MoS_2 nanosheets by pulsed laser deposition: An enhanced hydrogen evolution reaction,

Molecules, 2021, **26**.

21. Y. Yang, H. Wang, W. J. Qin, Y. X. Guo, H. Q. Yao, J. Li, K. R. Shi and S. L. Ma, MoS_2/Au^0/N-CNT derived from Au(III) extraction by polypyrrole/MoS_4 as an electrocatalyst for hydrogen evolution reaction, *J. Colloid Interface Sci.*, 2020, **561**, 298-306.
22. Y. K. Wen, H. Zhu, L. L. Zhang, S. G. Zhang, M. Zhang and M. L. Du, Activating MoS_2 by interface engineering for efficient hydrogen evolution catalysis, *Mater. Res. Bull.*, 2019, **112**, 46-52.
23. H. C. Tsai, B. Vedhanarayanan and T. W. Lin, Freestanding and hierarchically structured au-dendrites/3D-graphene scaffold supports highly active and stable Ni_3S_2 electrocatalyst toward overall water splitting, *Acs Appl. Energy Mater.* 2019, **2**, 3708-3716.
24. E. Topcu and K. D. Kiransan, Flexible gold nanoparticles/rGO and thin film/rGO papers: novel electrocatalysts for hydrogen evolution reaction, *J. Chem. Technol. Biotechnol.*, 2019, **94**, 3895-3904.
25. R. Bar-Ziv, P. Ranjan, A. Lavie, A. Jain, S. Garai, A. Bar Hen, R. Popoyitz-Biro, R. Tenne, R. Arenal, A. Ramasubramaniam, L. Lajaunie and M. Bar-Sadan, Au-MoS_2 hybrids as hydrogen evolution electrocatalysts, *Acs Appl. Energy Mater.* 2019, **2**, 6043-6050.
26. X. Zhao, D. W. He, Y. S. Wang and C. Fu, In situ growth of different numbers of gold nanoparticles on MoS_2 with enhanced electrocatalytic activity for hydrogen evolution reaction, *Chinese Phys. B*, 2018, **27**.
27. J. X. Zhang, T. Y. Wang, L. Liu, K. Z. Du, W. L. Liu, Z. W. Zhu and M. X. Li, Molybdenum disulfide and Au ultrasmall nanohybrids as highly active electrocatalysts for hydrogen evolution reaction, *J. Mater. Chem. A*, 2017, **5**, 4122-4128.
28. W. J. Zhou, T. L. Xiong, C. H. Shi, J. Zhou, K. Zhou, N. W. Zhu, L. G. Li, Z. H. Tang and S. W. Chen, Bioreduction of precious metals by microorganism: efficient gold@N-doped carbon electrocatalysts for the hydrogen evolution reaction, *Angew. Chem. Int. Ed.* 2016, **55**, 8416-8420.
29. G. Darabdhara, M. A. Amin, G. A. M. Mersal, E. M. Ahmed, M. R. Das, M. B. Zakaria, V. Malgras, S. M. Alshehri, Y. Yamauchi, S. Szunerits and R. Boukherroub, Reduced graphene oxide nanosheets decorated with Au, Pd and Au-Pd bimetallic nanoparticles as highly efficient catalysts for electrochemical hydrogen generation, *J. Mater. Chem. A*, 2015, **3**, 20254-20266.
30. Y. Yu, S. J. Lee, J. Theerthagiri, S. Fonseca, L. M. C. Pinto, G. Maia and M. Y. Choi, Reconciling of experimental and theoretical insights on the electroactive behavior of C/Ni nanoparticles with AuPt alloys for hydrogen evolution efficiency and Non-enzymatic sensor, *Chem. Eng. J.*, 2022, **435**.
31. T. Kwon, A. Yu, S. J. Kim, M. H. Kim, C. Lee and Y. Lee, Au-Ru alloy nanofibers as a highly stable and active bifunctional electrocatalyst for acidic water splitting, *Appl. Surf. Sci.*, 2021, **563**.
32. M. N. Hossain, S. Ahmad and H. B. Kraatz, Synthesis and electrochemical study of coinage metal nanodendrites for hydrogen evolution reaction, *Int. J. Hydrogen Energy*, 2021, **46**, 2007-2017.
33. M. A. Ehsan, D. Khalafallah, M. J. Zhi and Z. L. Hong, Synthesis of Au/Co_9S_8 composite aerogels by one-step sol-gel method as hydrogen evolution reaction electrocatalysts, *J.*

Porous Mater., 2021, **28**, 99-108.

34. X. L. Lu, T. S. Yu, H. L. Wang, R. C. Luo, P. Liu, S. L. Yuan and L. H. Qian, Self-supported nanoporous gold with gradient tin oxide for sustainable and efficient hydrogen evolution in neutral media, *J. Renew. Mater.* 2020, **8**, 133-151.
35. M. Y. Li, H. Liu, Y. H. Song and Z. Li, TiO_2 homojunction with Au nanoparticles decorating as an efficient and stable electrocatalyst for hydrogen evolution reaction, *Mater. Charact.*, 2019, **151**, 286-291.
36. F. Amiripour, S. N. Azizi and S. Ghasemi, Nano P zeolite modified with Au/Cu bimetallic nanoparticles for enhanced hydrogen evolution reaction, *Int. J. Hydrogen Energy*, 2019, **a44**, 605-617.
37. J. Wang, H. Zhu, D. N. Yu, J. W. Chen, J. D. Chen, M. Zhang, L. N. Wang and M. L. Du, Engineering the composition and structure of bimetallic Au-Cu alloy nanoparticles in carbon nanofibers: Self-supported electrode materials for electrocatalytic water splitting, *Acs Appl. Mater. Interfaces*, 2017, **9**, 19756-19765.
38. B. Zhang, H. Zhu, M. L. Zou, X. R. Liu, H. Yang, M. Zhang, W. W. Wu, J. M. Yao and M. L. Du, Design and fabrication of size-controlled Pt-Au bimetallic alloy nanostructure in carbon nanofibers: a bifunctional material for biosensors and the hydrogen evolution reaction, *J. Mater. Sci.* 2017, **52**, 8207-8218.
39. M. Zhang, S. S. Wang, T. Li, J. D. Chen, H. Zhu and M. L. Du, Nitrogen and gold nanoparticles co-doped carbon nanofiber hierarchical structures for efficient hydrogen evolution reactions, *Electrochim. Acta*, 2016, **208**, 1-9.